Engineering and Technology Journal
Journal homepage: https://etj.uotechnology.edu.iq

Experimental adsorption of drug loading for nano-carriers

Hind H. Abbood[a*], **Alaa A. Abdul-Hamead**[b], **Farhad M. Othman**[b]

[a] Training and Workshops Center, University of Technology-Iraq, Alsina'a street, 10066 Baghdad, Iraq.
[b] Materials Engineering Dept., University of Technology-Iraq, Alsina'a street, 10066 Baghdad, Iraq.
*Corresponding author Email: Hind.h.abbood@uotechnology.edu.iq

HIGHLIGHTS

- Mesoporous silica nanoparticles (MSNs) with tunable pore sizes were developed for drug delivery applications
- Enhanced paclitaxel (PTX) loading and pH-responsive release were achieved
- Higher PTX release was demonstrated in acidic cancer conditions compared to physiological pH

ARTICLE INFO

Keywords:
Nanomedicine
Drug delivery systems
Mesoporous silica nanoparticles
Paclitaxel drug
Dialysis method

ABSTRACT

This study focuses on preparing and characterizing mesoporous silica nanoparticles (MSNs) with two distinct pore sizes: small and large. The MSNs were employed to encapsulate paclitaxel (PTX), achieving enhanced drug-loading capacity and improved cytotoxicity. The MSNs synthesis by modified sol-gel method and the pore size can be modified by adding the mesitylene to MSNs for 1, 3, and 5hr. The drug loading was carried out by dissolving the PTX drug with different solvents, water, ethanol, DMSO, and dichloromethane by the Adsorption method and measuring the drug loading capacity and drug loading efficiency for both types of mesoporous silica nanoparticles. All MSNs were characterized by transmission electron microscopy (TEM), Fourier transform infrared spectroscopy (FTIR), N_2 adsorption isotherms, scanning electron microscopy (SEM), and X-ray diffraction (XRD) analysis for determination of their characterizations. In-vitro, The effects of pore sizes of MSNs on the loading of PTX and its release from MSNs were conducted at two pH conditions: pH= 7.4 and 5.5 as representative of physiological and cancer environment conditions. The released PTX from PTX-loaded MSNs into the pH of the physiological environment was slower than that into the cancer environment. The release of PTX was strongly pH-dependent on the selected media.

1. Introduction

Nanomedicine is the application of nanotechnology to the prevention and treatment of diseases in humans is a relatively new field of science that includes physics, chemistry, materials engineering, biology, and medical science. Nanomedicine is crucial in advancing healthcare strategies, particularly in imaging, disease diagnosis, tissue engineering, and drug delivery systems [1-3]. Drug delivery is one of the most active research areas in nanomedicine for treating diseases. It will create a dose difference between the target site and the rest of the body, enhance the effectiveness of treatment in the target area, and reduce side effects on the rest of the body. Nano-delivery systems are a r

elatively new and rapidly evolving science in which Nano-scale carriers deliver drugs to specific target sites in a controlled manner or act as diagnostic tools [4]. The engineered drug delivery systems are considered one of the most promising tools in cancer treatment. Developing and applying these systems can increase the solubility and permeability of antitumor drugs, enhance the retention effect, prolong the circulation half-life, improve biological distribution, and reduce toxicity. Low permeability and poor water solubility are limitations of conventional drug delivery [5]. Drug Delivery Systems (DDSs) protect the drug from rapid degradation or clearance and enhance drug concentration at target sites. Therefore, lower doses of the drug are required. Drug release from these DDSs can be controlled by diffusion, swelling followed by diffusion, and erosion in a time-dependent manner [6]. Ceramic nanocarriers are inorganic systems with or without porous features that can be easily engineered for optimal size, shape, and porosity, making them cost-effective drug delivery agents. Many studies have been made on common biocompatible ceramic nanoparticles such as silica, titania and alumina [7].

Porous materials are a type of engineering material with nano-scale pores. Porous Nanomaterials exhibit unique properties compared to solid particles of the same size, such as lower density, larger active surface area, desired permeability, good selectivity, higher drug effectiveness, better in vivo balance of drug concentration in the body, and more convenience to the patient. For this

http://doi.org/10.30684/etj.2024.154925.1840
Received 01 November 2024; Received in revised form 25 December 2024; Accepted 27 December 2024; Available online 29 January 2025
2412-0758/University of Technology-Iraq, Baghdad, Iraq

purpose, the encapsulation of drugs on porous particles has been proposed [8]. There are three primary categories depending on the sizes of their pores: Microporous (<2 nm), Mesoporous (2–50 nm), and Macroporous (>50 nm). Mesoporous materials are more efficient than the other types due to their expansive surface areas, elevated porosity, adjustable pore dimensions, and exceptional thermal characteristics. These attributes empower these substances to accommodate substantial quantities of payload molecules, safeguard them against premature deterioration, and facilitate controlled and rapid release, exemplified by mesoporous geopolymer, mesoporous MgO, mesoporous SiO_2, mesoporous TiO_2 mesoporous ZrO_2, and so forth [9].

Mesoporous Silica Nanoparticles (MSNs) belong to the category of structured mesoporous bioceramics. Their distinctive features, such as their precisely defined internal arrangement with large pore volume (ranging from 0.6 to 1 cm^3 /g), large surface area (varying from 700 to 1000 m^2 /g), adjustable size (ranging from 50 to 200 nm), and shape and easy surface modification, make them ideal platforms for the design of Nanocarriers [8]. In the field of cancer, MSNs are emerging with therapeutic potential for targeted drug delivery in chemotherapeutics. MSNs can also improve the bioavailability of poorly soluble drugs by converting them into Mesoporous structures. Unique to MSNs are the encapsulation of the drug, crystallization of the drug in its Mesopores, and greater dispersion with greater surface area and solubility. Its shape and surface can be customized, offering many options for loading anti-cancer drugs such as docetaxel and doxorubicin [10]. Mesoporous silica nanoparticles have low toxicity and high drug-loading capacity, so they are used in controlled and targeted drug-delivery systems. Basically, silica is widely present in the environment, from unicellular organisms to higher plants. It has comparatively better biocompatibility than other metal oxides like titanium and iron [11]. MSNs induced substantially lower hemolytic effects than nonporous silica NPs because of the reduced silanol density due to the presence of mesopores. At the same time, silanol groups in silica can show affinity with phospholipids, which can be actively absorbed by cells [12]. The engineered Drug delivery systems are considered one of the most promising tools in cancer treatment. Developing and applying these systems can increase the solubility and permeability of antitumor drugs, enhance the retention effect, prolong the circulation half-life, improve the biological distribution, and reduce toxicity. Low permeability and poor water solubility are limitations to conventional drug delivery, as illustrated in Figure 1 [13].

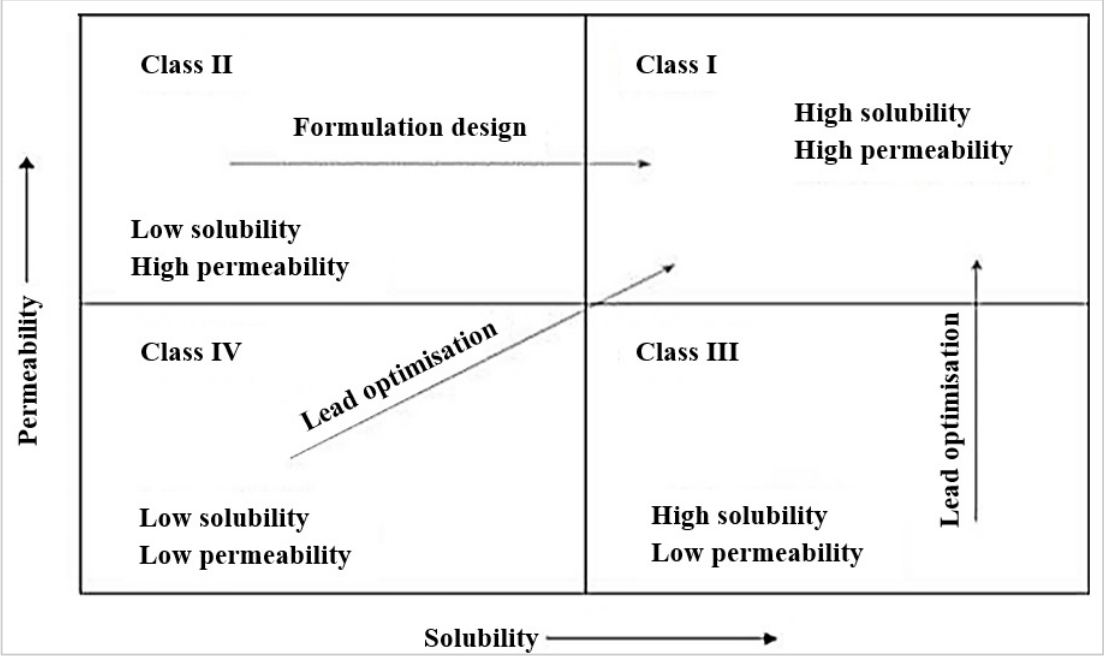

Figure 1: Biopharmaceutics classification system (BCS) classification of drug [14]

Paclitaxel, or taxol, a taxane drug, is a highly successful anti-cancer drug derived from plants. In 1992, PTX was approved by the Food and Drug Administration (FDA) for the treatment of ovarian, breast, and lung cancer with good clinical results [15,16]. Taxol (BCS Class: IV), a low-water-solubility anticancer drug, is formulated using Cremophor EL and ethanol, but it causes unwanted side effects. The Nano-formulation of paclitaxel eliminates the need for these solvents, reducing side effects. Paclitaxel is a white to off-white crystalline powder with the molecular formula $C_{47}H_{51}NO_{14}$. It is insoluble in water, has a melting point near 216 °C, and is highly lipophilic. The generally accepted dose is 200-250 mg/m^2 given as 3- hour and 24-hour infusions. The terminal half-life is 1.3-8.6 hours (average 5 hours) [17]. Most MSNs are synthesized using a modified Stober method, often referred to as the sol-gel method, which has been widely studied in the synthesis of various inorganic compounds.

The synthesis of MSNs can use a variety of mechanisms and it consists of three basic steps including i) a sol-gel process to generate silica, ii) surfactants as structure-directing agents to prepare mesoporous materials; liquid crystal templates Mechanism, and iii) Modified dilute-state Stöber method for the preparation of spherical nanoparticles [18].

MCM-41 is the most widely studied MSN type for biomedical applications. Use the surfactant cetyltrimethylammonium bromide (CTAB) as the liquid crystal template, tetraethyl orthosilicate (TEOS) or sodium metasilicate (Na_2SiO_3) as the silica precursor, and alkali as the catalyst [19]. In Adsorption method, Adsorption is a widely used method for loading drugs into mesoporous materials (MSNs) using concentrated drug solutions. The slurry fills the mesopores by capillary action. The drug-

loaded MSNs are recovered by filtration or centrifugation. This is a widely used method that can be applied to drugs across all four BCS classes [20]. Dialysis methods are frequently used to determine nanoparticle drug delivery systems in vitro drug release profiles. The drug release profile generated from dialysis-based assays has been widely used to guide formulation development, facilitate quality control and regulatory filing, and, in the best-case scenario, establish the in vitro-in vivo correlation (IVIVC) of the nanoparticle formulation [21,22]. This study investigated the potential of MSN as nanocarriers for human plasma blood delivery of PTX because PTX is a natural anticancer and pH-sensitive drug with side effects on noncancerous cells.

2. Experimental

2.1 Materials and equipment used

Materials and the equipment that have been used in the experimental work with their suppliers in this study for the synthesis of nanoceramics carriers are mentioned in Table 1.

Table 1: Used materials

NO	Materials and equipment	Suppliers	Origin
1	CTAB	Himedia chemicals	India
2	TEOS	ALORICH	China
3	NaOH	DAEJUNG (CHEMICALS & METALS)	South Korea
4	Deionized water	----------	----------
5	mesitylene	Himedia chemicals	India
6	Paclitaxel	Hangzhou Hyper Chemicals Limited	China
7	Dichloromethane	SCRC	China
8	Methanol	SCRC	China
9	Ethanol	SCRC	China
10	DMSO	SCRC	China
11	magnetic stir	M TOPE	Korea
12	vacuum filter	Hettich centrifuges	Germany
13	Furnace	Schneider Electric	French
14	vacuum oven	TYFSF	China
15	Centrifuge	Hermal	Germany
16	pH meter	Lab India Instruments Ltd	India
17	Digital weighing Machine	Sartorius	Germany
18	Ultrasonic Cleaner	Skey men	China
19	Pipette	----------	----------

2.2 Synthesis of MSN with different pore sizes

Following recorded procedures, two types of mesoporous silica nanoparticles, small (S-MSNs) and large(L-MSNs) pores, were prepared with a little modification. For S-MSNs, the solution of 480 mL deionized water and NaOH (aq) (2M, 3.5 mL), (1.0 g, 2.7 mmol) of Cetyltrimethylammonium bromide (CTAB) was stirred vigorously at 1000 rpm for 5 h at 80 ℃ in the bottom round flask. Then, dropwise tetraethyl orthosilicate (TEOS) (5.0 mL, 22.56 mmol) was added by pipette at a 1 mL/ min rate. The mixture was vigorously stirred for another 2 h at 80 °C. The resulting white precipitate was filtered by a vacuum filter, washed with plenty of methanol to remove partial surfactant, and dried at room temperature. For L-MSNs, the (7.0 mL, 50.30 mmol) of mesitylene were added to the solution with CTAB, which expanded the pores of MSNs by 5hr. Then, using the calcination in the furnace, the surfactant template was removed at 550 °C for 6 h with a heating rate of (1-2 °C/min). Lastly, white powder of S-MSNs and L-MSNs was produced.

2.3 Drug loading study

An adsorption method was utilized for PTX loading. Drug loading is typically accomplished by soaking a drug solution with MSNs to allow adsorption through interaction between the drug and the particle surface. Hydrogen bonds and electrostatic attractions mediate this interaction. Before using MSNs for drug loading, 200mg of S-MSNs and L-MSNs were kept in the oven at 80 ℃ for 30 min to remove the moisture from the mesostructure's pores and obtain maximum saturation for PTX loading. PTX solution is prepared by dissolving 100 mg of PTX with 10 ml of different solvents, water, ethanol, DMSO, and dichloromethane in a sonicator to obtain clear and concentrated drug solutions. After that, S-MSNs and L-MSNs were soaked with paclitaxel solution for drug loading after agitating under closed and light-sealed conditions for different intervals (1, 2, 4, 8, 16, 24) h at 25 ℃ and 400 rpm. The supernatants were measured using high-performance liquid chromatography (HPLC) to assess the amount of unentrapped drugs. Drug-loaded MSNs were centrifuged at 10,000 rpm for 30 min and, washed with deionized water to remove residue, and separated again with a centrifuge device; the product was dried in a vacuum furnace, resulting in the white powder from PTX@S-MSNs and PTX@L-MSNs.

$$\text{PTX loading efficiency(LE\%)} = \frac{\text{(Total PTX – unloaded PTX)}}{\text{Total [PTX]}} \times 100 \quad (1)$$

$$\text{PTX loading capacity(LC\%)} = \frac{\text{(Total PTX – unloaded PTX)}}{\text{amount of PTX loaded in MSNs}} \times 100 \quad (2)$$

3. MSNs characterization

The SEM is a powerful technique for analyzing the structure and morphology of the prepared S-MSNs and L-MSNs using scanning electron microscopy (FEI INSPECT F50, origin: USA) with an accelerating voltage of (20 kV). The powders were plated with gold before the SEM observation. EDX analysis was utilized in this study to identify the chemical composition of prepared powder and ensure the specimens were without CTAB and mesitylene. The specific surface area and the total pore volume for S-MSNs and L-MSNs were obtained by using nitrogen adsorption isotherms (Brunauer, Emmett, and Teller method) on a surface area analyzer (Type: TriStar II Plus, Origin: USA). The X-ray diffraction was used to find the crystalline structure, identify crystalline phases, orientation and determine structural properties of the prime MSNs and PTX@MSNs with 2Θ in the range from 10 ° to 80 ° with scan rate 10 (deg./min) with a step size of 0.02° and an accumulation time of 5 s. For this purpose, the diffractometer was equipped with X-ray Tube cu (λ = 1.54060 Å) operating at 40 kV and 30 mA.

The X-ray diffract meter (Panalytical X' Pert, Pr, UK) did the XRD test. TEM Analysis confirmed the porous framework and particle size of MSNs and coating MSNs. TEM images of MSNs and coating MSNs specimens were taken with a (Tem philips em208s) with 100 kv. The FT-IR instrument is used to analyze the chemical bonds and the functional groups of prime MSNs and PTX-MSNs in the range between (4000-400 cm^{-1}). This equipment's types (Thermo Fisher Scientific/ USA). Zeta potential was carried out by electrophoretic mobility using Zeta sizer Nano ZS (BROOKHAVEN, origin: USA) at 25 °C in deionized water solution for prime MSNs and PTX-MSNs specimens. HPLC equipment separates, identifies, and quantitates compounds in liquid samples. HPLC [Knuaer, Origin: Germany] system consisted of a Binary high-pressure gradient pump [P6.1L, Knuaer, origin: Germany], Sample loop (20 µl), and injector [D1357, Knuaer, origin: Germany], Diode array UV detector [DAD 2.1L, Knuaer, origin: Germany], Analysis and system control software [Claritychrom, V 7.4.2.107, Dataapex, origin the Czech Republic], The separation on C18 column (Knuaer, Germany) (250 - 4.6 mm i.d., 5 µm particle size, 80 Å pore size); mobile phase: Acetonitrile–water (70:30, 0.1% trifluoroacetic acid); flow rate of the mobile phase: Flow rate: 1 ml /min; the UV detector Wavelength (λ max) =228 nm for drug loading and release study.

4. In vitro drug release study

4.1 Standard calibration curve preparation

The calibration curves for PTX were established using a methanol solution. A stock solution with a concentration of 2 mg/ml was prepared, and from this, a series of PTX dilutions with varying concentrations ranging from 1 to 200 µg/ml were created. PTX detection was performed by matching the retention time and absorbance spectrum of each PTX standard. HPLC analysis was conducted at the wavelength corresponding to the maximum absorbance of PTX (λ max= 228 nm). The concentration of PTX in the samples was determined by relating the serial concentrations of external standard materials to their respective peak areas, allowing the construction of a calibration curve correlating concentration with peak area.

4.2 In-vitro drug release

An in vitro study of PTX release from drug-loaded MSNs has been calculated using a dialysis bag (12000 MWCO) to replicate natural and tumor environments in two media for phosphate-buffered saline (PBS) with a pH of 7.4 and 5.5. Due to the low water solubility of PTX, 0.1% Tween 80 was applied to the release media to induce a sinking state. In short, all the media were dispersed by 5 mg PTX@. The dispersed MSNs were shaken in a shaker state at condition 37 ℃ and rate of 100 rpm. It was centrifuged for 10 minutes at 17000 rpm at the predetermined sampling time, followed by the separate supernatant. Moreover, MSNs have been suspended while keeping their sink status by adding sufficient new media to preserve their release profile. In addition, PTX supernatant amounts have been calculated by the HPLC and based on the 0.22 µm membrane-filter calibration curve after filtration.

5. Results and discussion

5.1. Characterization techniques

5.1.1 Scanning electron microscopy (SEM) and energy dispersive X-ray (EDX) analysis

The surface morphology of synthesized S-MSN and L-MSN nanoparticles was studied using scanning electron microscopy (SEM), as depicted in Figure 2. The SEM images demonstrated the formation of almost spherical silica nanoparticles with an average particle size of about (177 nm) and porous structure (rough surface nature) agglomerated in clusters, as shown in Figure 2 (a). The addition of mesitylene to the starting solution led to the form of spherical and quasi-spherical porous silica nanoparticles with bigger particle sizes of about (354.65 nm), with more rough surfaces compared with the particles surfaces before adding the mesitylene, as shown in Figure 2 (b). SEM images indicated that the addition of mesitylene affected the shape and size of the prepared silica nanoparticles to obtain larger particles. Energy dispersive X-ray analysis (EDX) was carried out to determine the chemical composition of prepared samples. Figure 3 (a, b) showed the EDX spectra for (S-MSNs) and (L-MSNs) samples. The obtained EDX peaks improved the samples' chemical composition, including the characteristic peaks of silicon and oxygen elements. Tables 2 and 3 presented the atomic and weight ratios of silicon and oxygen within the (S-MSNs) and (L-MSNs) samples, respectively. Silicon forms the base that binds to oxygen atoms to create a mesh-like

network. On the other hand, the characteristic peak of the gold element is attributed to the gold coating process of the samples before the EDX test [23, 24].

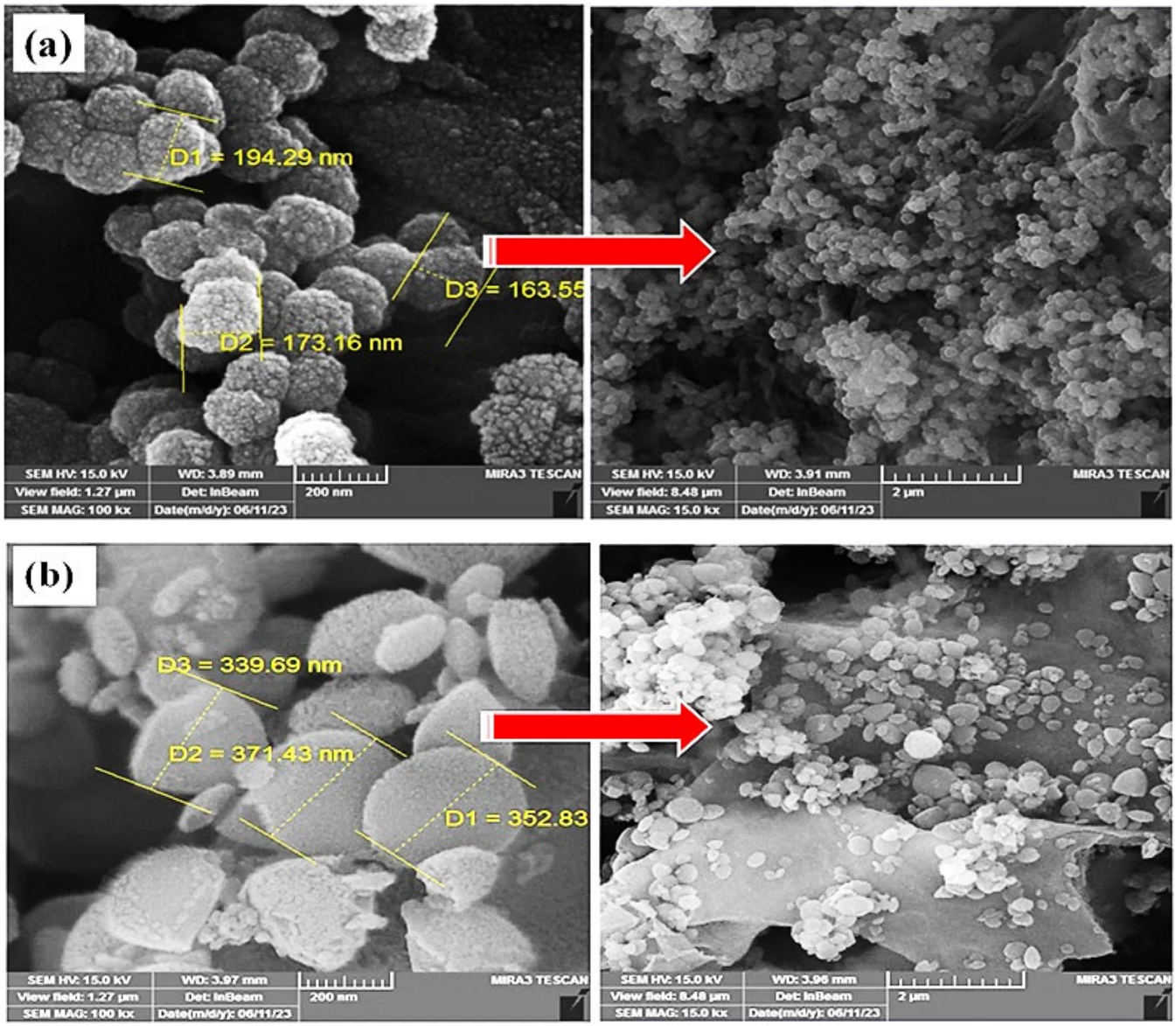

Figure 2: SEM images of porous silica nanoparticles (a) S-MSN (b) L-MSN

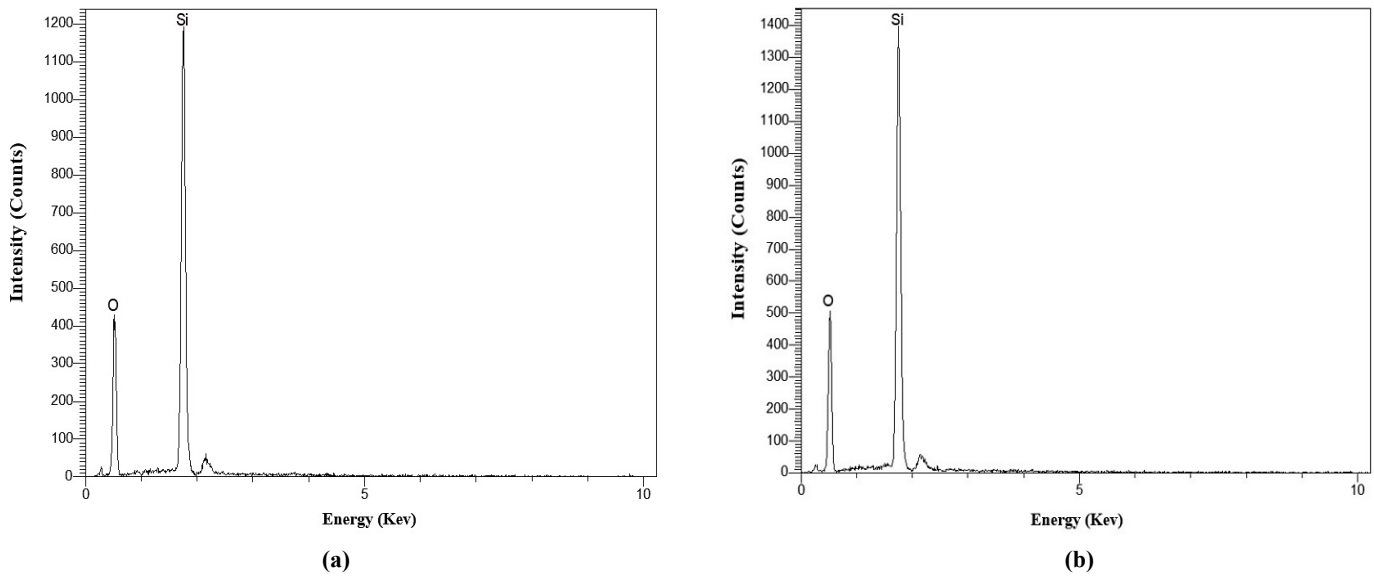

Figure 3: EDX spectra of prepared mesoporous silicon (a) S-MSNs (b) L-MSNs

Table 2: Represents the element ratios of small mesoporous silicon S-MSNs

Element	Weight (%)	Atomic (%)	Error (%)
O	53.01	66.45	2.0184
Si	46.99	33.55	2.7402
	100.00	100.00	

Table 3: Represents the element ratios of large mesoporous silicon L-MSNs

Element	Weight (%)	Atomic (%)	Error (%)
O	53.30	66.71	1.5035
Si	46.70	33.29	2.5435
	100.00	100.00	

5.1.2 Transmission electron microscopy (TEM)

TEM was carried out to investigate the morphological nature of the prepared samples. Figures 4 (a and b) and Figure 6 (a and b) showed the obtained TEM images of S-MSNs and L-MSNs. The TEM images demonstrated that the prepared mesoporous silica nanoparticles were mono-distributed nanoparticles with a spherical shape, the mean particle size of S-MSNs is (30 nm) while for L-MSNs is (58 nm), as shown in Figure 4 (a and b). The obtained TEM images exhibited the honeycomb porous structure of S-MSNs and L-MSNs samples.

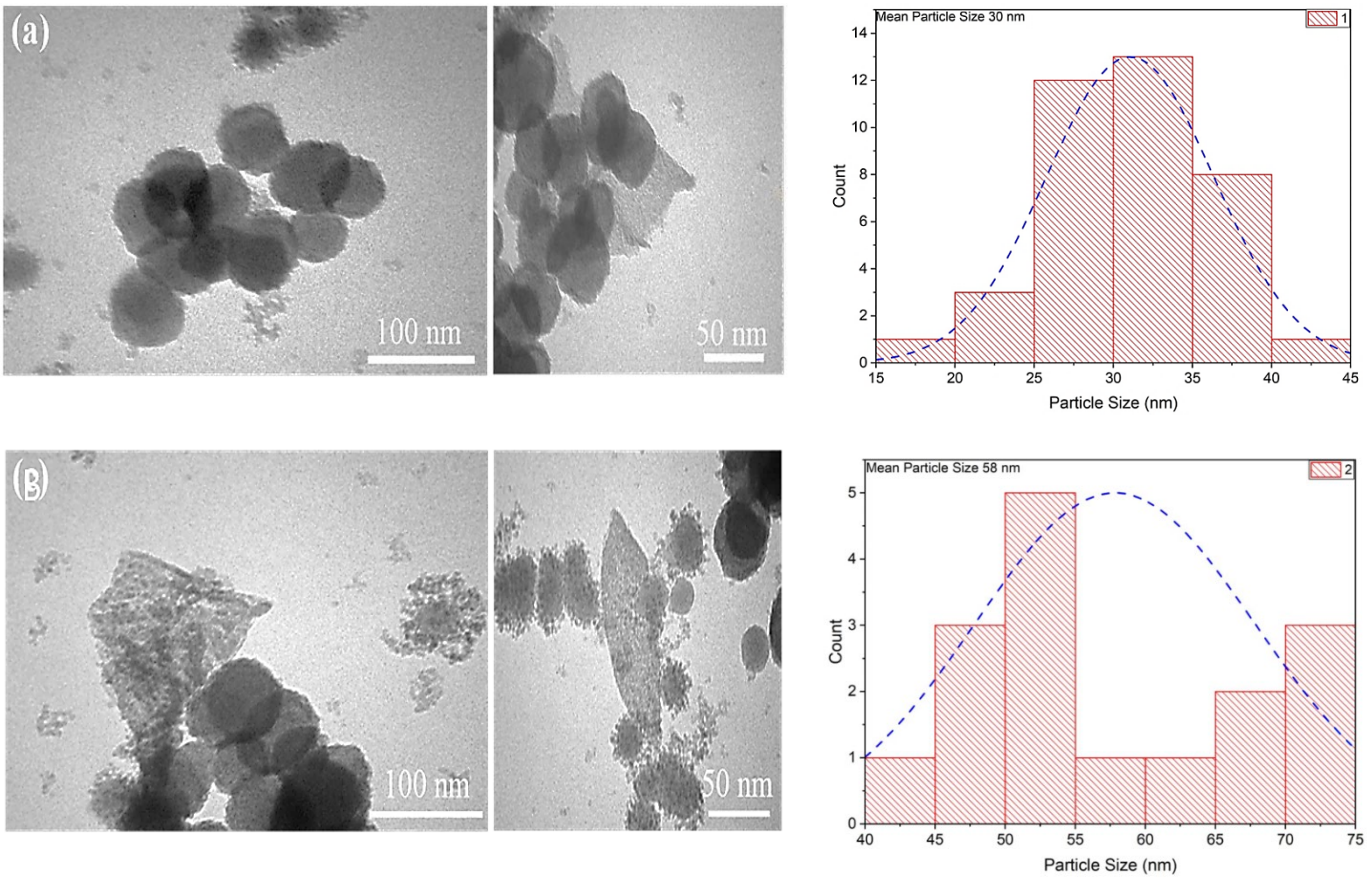

Figure 4: Transmission electron microscopy (TEM) images of prepared mesoporous silicon nanoparticles (a) S-MSNs and (b) L-MSNs

5.1.3 BET/BJH analyzer

A reliable method for studying the porosity of mesoporous materials is nitrogen adsorption and desorption analysis. Prior to characterization, a single sample of MSNs was degassed for 5 h under vacuum at 200 °C. The BET-specific surface area was measured using a BET method for isothermal treatment. By applying the Barrett – Joyner – Halenda (BJH) method to the isotherm, the pore volume and pore diameter of plain MSNs were determined.

5.1.3.1 Brunauer–emmett–teller (BET) exam

The nitrogen adsorption-desorption isotherm was carried out of S-MSNs and L-MSNs samples, in order to investigate the specific surface area, pore volume, and pore size of prepared samples. Figure 5 (a, b) presented the nitrogen adsorption and desorption isotherm curves of S-MSNs and L-MSNs respectively. The obtained adsorption-desorption curves of S-MSNs and L-MSNs correspond to the type IV adsorption isotherm with hysteresis loop at a high value of pressure (P/P_o = 0.8 - 1), which is the characteristic curves of mesoporous material.

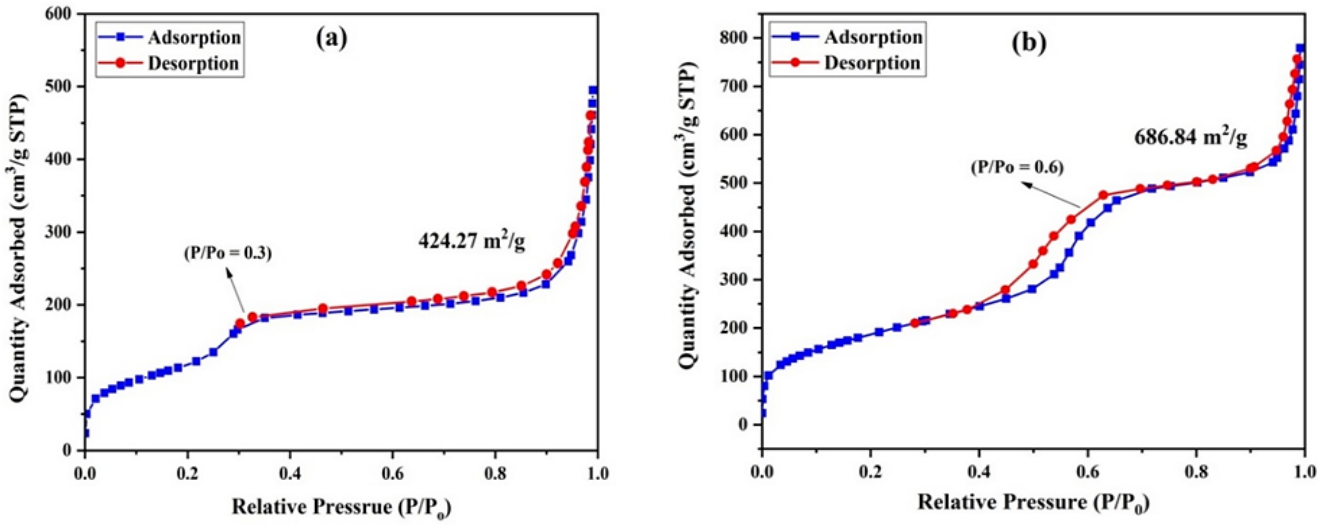

Figure 5: Brunauer–emmett–teller (BET) (surface area analysis): Nitrogen adsorption - desorption isotherm curves of (a) S-MSNs and (b) L-MSNs samples

The hysteresis loop of samples at a relative pressure (P/P_o = 0.3 – 0.8) is identical to the hysteresis loop type H1, which is attributed to cylindrical pores, while the curves of samples at higher pressure are typical to hysteresis loop type H3, which referred to the slit-shaped pores. The mixture of cylindrical and slit-shaped pores is due to that the surfactant CTAB is able to form both spherical and oblate micelles depending on the oxyethylene chains arrangement within the micelles. Observed that the adsorption curves of samples characterized by knees above the relative pressure (P/P_o = 2.2), which attributed to the adsorption followed by capillary condensation process of the gas molecules. The specific surface area of S-MSNs is (424.27 m^2/g), which is smaller than that of the L-MSNs (686.84 m^2/g) as mentioned in Figure 4 (a, b) [25-30].

5.1.3.2 Barrett- joyner - halenda (BJH) exam

Figure 5 (a, b) presents the BJH pore volume curves as a function of pore size curves (BET) of S-MSNs and L-MSNs samples. The results demonstrated that the pore size of S-MSNs and L-MSNs were (2.5 nm) and (3.2 nm) respectively. The mesoporous silicon sample exhibited narrow pore size distribution which proved homogeneous material reduction, as depicted in Figure 6 (a, b) [27, 29]. The nitrogen adsorption-desorption isotherm curves of S-MSNs and L-MSNs still exhibited a type H1 followed by a type H3 hysteresis loop. This behavior mentions that the metallic silicon keeps part of the mesopores, although some pore shrinkage was detected in the pore size distribution, as shown in Figure 6 (a, b). The strong H3 loop of samples as shown in Figure 4 (a, b) can be attributed to the slit-shaped pores created between Silica crystals [28-30].

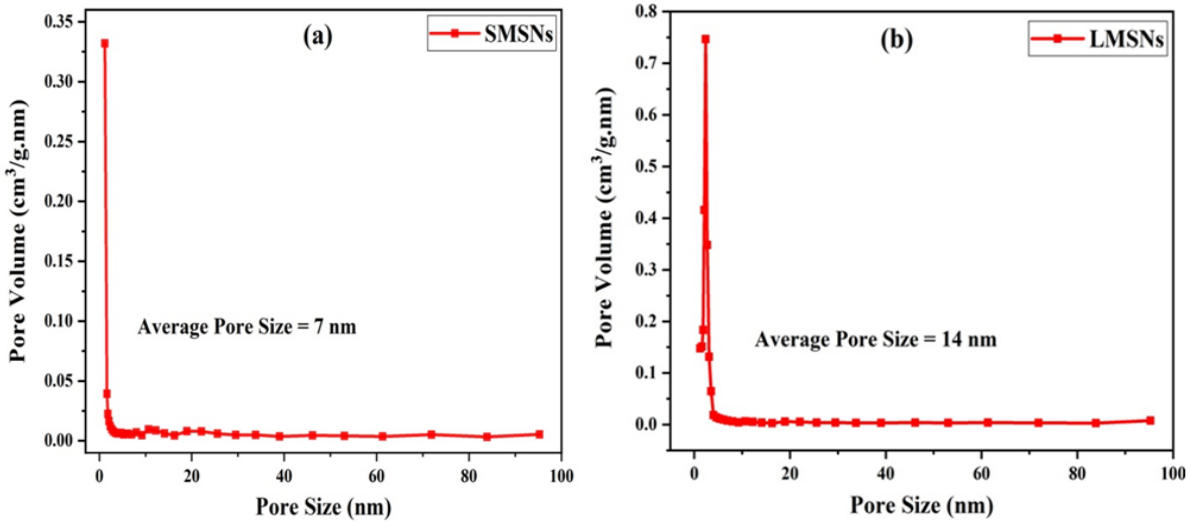

Figure 6: BJH pore volume vs. pore size curves (BET) of (a) S-MSNs and (b) L-MSNs

5.1.4 X-ray diffraction (XRD)

XRD was carried out to determine the crystalline structure of prepared porous silicon samples using (a Shimadzu XRD-6000 powder) diffractometer. Figure 7 shows the XRD patterns of pure and PTX-loaded porous silicon samples. The obtained XRD patterns obtained XRD patterns confirmed the amorphous crystalline structure of all pure and PTX-loaded silicon samples. The results showed that the XRD patterns of all samples with a broad peak at ($2\Theta = 22.1^{o}$), which attributed to the amorphous structure of silica nanoparticles, corresponded to the standard data (96-101-0939), the XRD patterns agreed with

the SEM and TEM results. There is no noticeable difference detected between the XRD patterns for pure and PTX-loaded samples, which indicated the similar structures of silica nanoparticles [31,32].

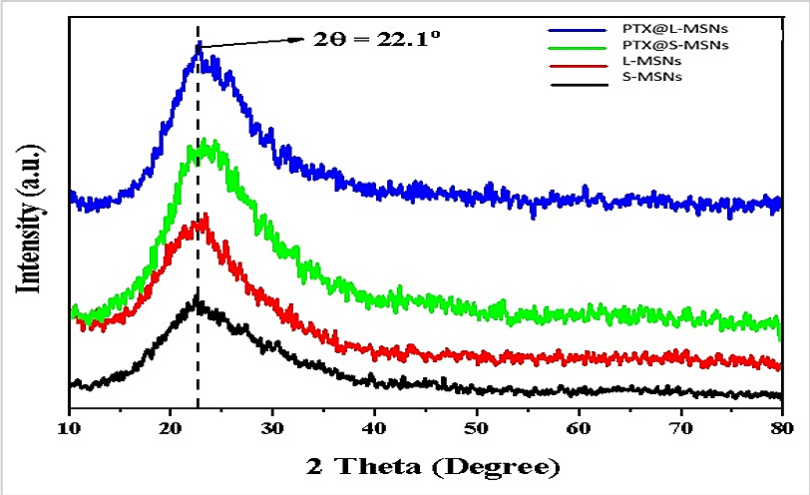

Figure 7: XRD patterns of prepared porous silica nanoparticle samples

5.1.5 Fourier-transformed infrared spectra (FTIR)

The FTIR spectroscopy test was carried out to determine the functional groups within the prepared porous silica samples, using an FTIR spectrometer (SHIMADZU - FTIR 8400) in the range (500 – 4000 cm^{-1}). Figures (8 and 9) presented the obtained FTIR spectra curves of small mesoporous silica (S-MSNs) and large mesoporous silica (L-MSNs) samples, the examined samples were pure S/LMSNs, and loaded PTX-S/LMSNs.

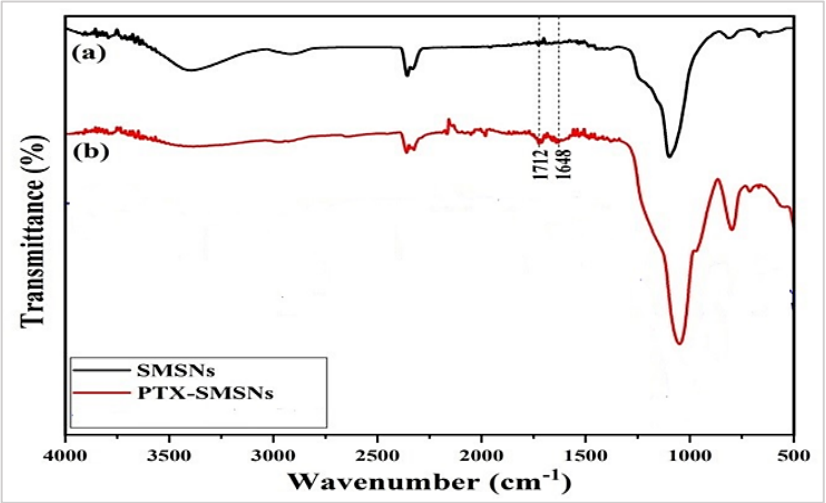

Figure 8: FTIR spectra curves of prepared samples (a) S-MSNs (b) PTX@S-MSNs

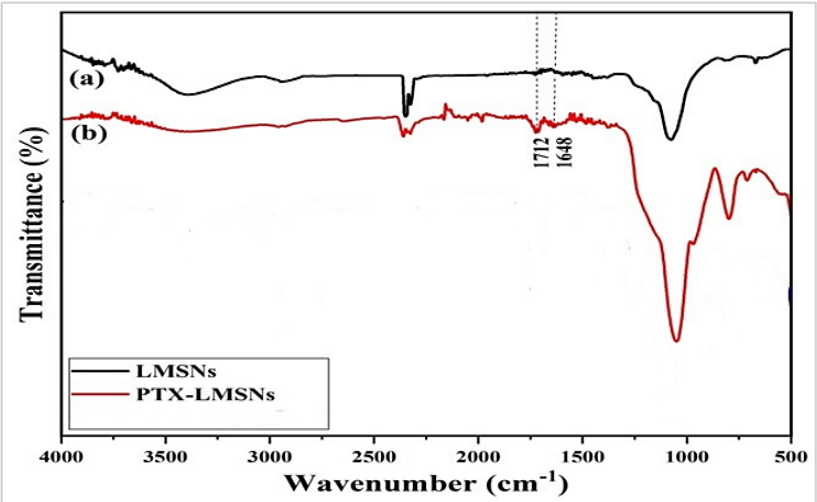

Figure 9: FTIR spectra curves of prepared samples (a) L-MSNs (b) PTX@L-MSNs

From Figures 8 (a) and 9 (a), the strong broad absorption band at 1050 cm^{-1} is attributed to stretching vibrations of the Si-O-Si bond with a shoulder at 984 cm^{-1}, while the vibrations bands centered at 708 cm^{-1}, 800 cm^{-1}, 2345 cm^{-1} and 3409 cm^{-1} assigned to O_n-Si-H_x bond deformation [33-35]. The characteristic bands at 1712 cm^{-1} and 1648 cm^{-1} attributed to C=O and C-C stretching vibrations bands respectively of the paclitaxel drug [36,37]. The FTIR spectrum of (PTX-S/LMSNs) showed that when the paclitaxel medicine loaded on the mesoporous silica led to an increase in the width of the strongest absorption band at 1050 cm^{-1} of the Si-O-Si bond. As a result of the overlapping with the characteristic bands of paclitaxel medicine at 1245 cm^{-1} and 1074 cm^{-1} that attributed to the C-N and C-O stretching vibrations [38], as presented in Figures 8 (b) and 9 (b). All these FTIR results confirmed the successful fabrication of paclitaxel-loaded mesoporous silica (PTX-S/LMSNs). Observed that the peaks at 708 cm^{-1} and 984 cm^{-1} became clear and sharp after the addition of (PTX), which can be attributed to the oxidizing process of the mesoporous silica. From the obtained results, it was found that there is no appreciable difference between the FTIR spectra of prepared large and small mesoporous silicon [39].

5.1.6 Thermo gravimetric analysis (TGA)

The thermogravimetric analysis (TGA) was carried out on prepared samples to investigate the decomposition behavior (decomposition temperature) within the heating process of the samples in air. Figure 10 presents the TGA and DTA curves of prepared samples. The results demonstrated that the pure S-MSNs and L-MSNs samples started to increase in weight at the temperature (150 °C and 250 °C), which was attributed to the partial oxidation process of mesoporous silica nanoparticles [40], to reach (1.610 % and 1.9 %) respectively of the original weight at the temperature (900 °C), while the samples exhibited weight loss at low temperature due to the releasing of the absorbed environmental moisture [41], as shown in Figure 10 (a, c). From Figure 10 (b, d), the samples S-MSNs and L-MSNs loaded with PTX demonstrated a weight loss at a low-temperature range (60 °C to 150 °C) due to the removal of moisture, and this weight loss continues clearly within the temperature range (250 – 380 °C), which is attributed to the paclitaxel degradation at this temperature (250 °C) [42]. Then the SMSNs and LMSNs nanoparticles immediately began to oxidize, which led to a clear increase in weight percentage (17.6%, 17%) respectively. The total weight loss of S-MSNs and L-MSNs samples of 21.15% and 5.98% respectively. The results revealed that weight loss up to 400 °C becomes constant until temperature of 900 °C.

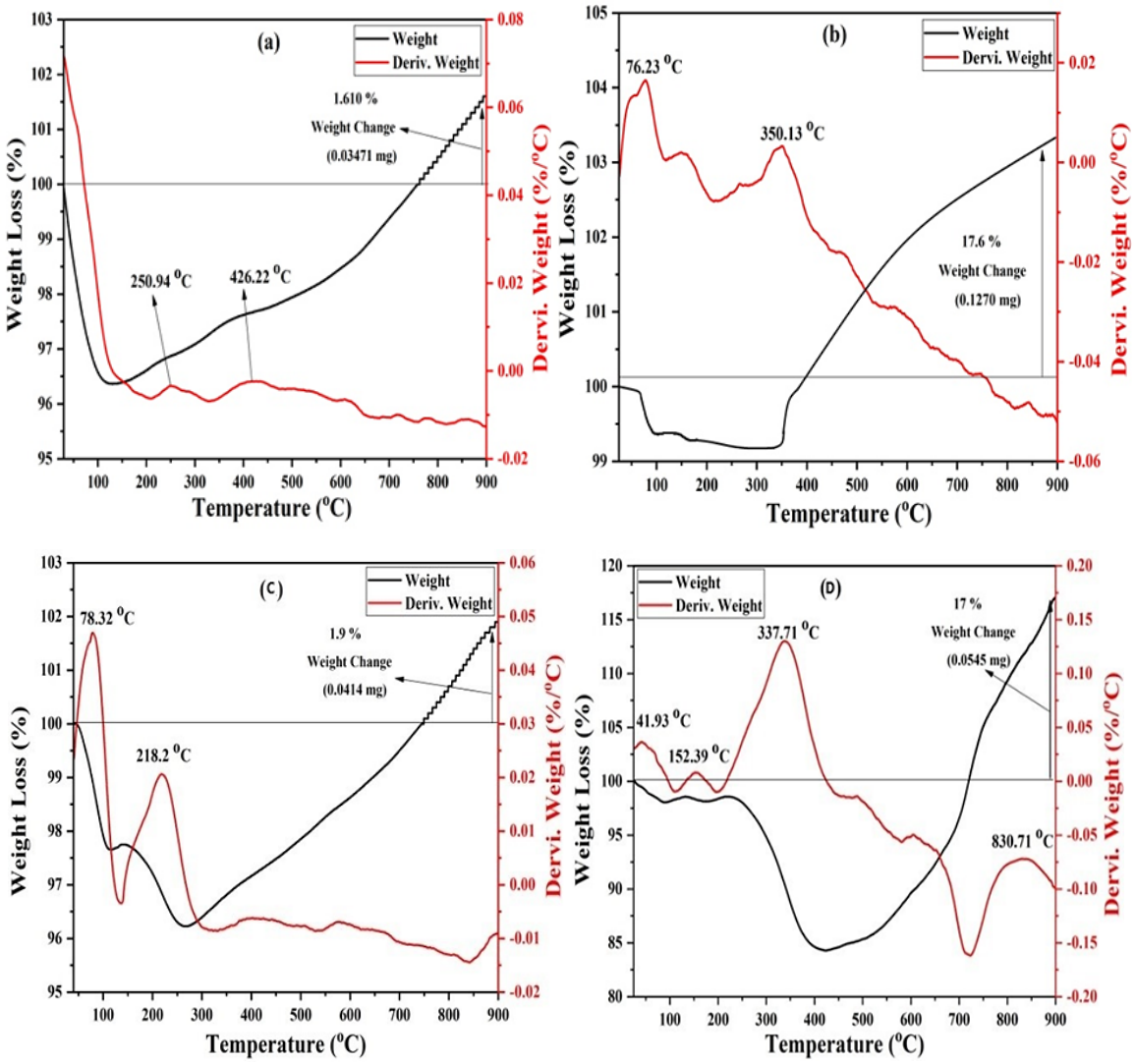

Figure 10: TGA and DTA curves of prepared samples (a) S-MSNs (b) PTX@S-MSNs (d) L-MSNs (e) L-PTX@MSNs

5.2 Drug loading study

The MSNs appeared to have accessible mesopores as indicated in TEM images and N_2 adsorption-desorption analyses, hence they were used as drug carriers for the water-insoluble drug PTX using the adsorption method. The loading of PTX into the MSNs is also controlled by the chemical nature of the size, pores, and shape of the nanoparticles, which may be related to electrostatic interactions. The inorganic networks of MSNs have a large number of silanol groups (Si-OH), which interact with the functional group of PTX drug by means of hydrogen bonding on the mesopore surface. Interaction between the MSNs silanol group and the drug functional group was attractive, the drug molecules either confined within the pores or they adsorbed to the surface of MSNs. The probable mechanism of drug loading is that the H group of amine or carboxyl and hydroxyl group of PTX will form hydrogen bonds to the group of silanol as shown in Figure 11 of developed mesoporous silica nanoparticles, and the drug molecules will then be retained in the mesopores.

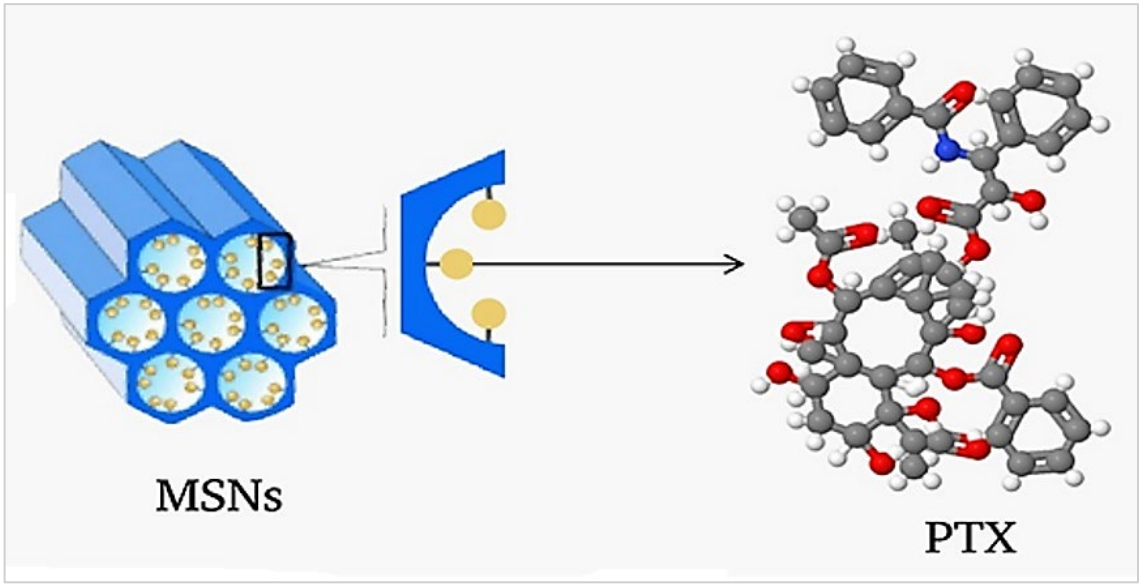

Figure 11: Adsorption of PTX drug on mesopores of MSNs

5.2.1 Drug characterization

The drug melting point was measured by the Electrothermal melting point apparatus, according to USP 741, and was found to be 218 ℃. This result was aligned with the reported values which might indicate the purity of the powder sample used in the study [43]. The drug scanned in methanol with a HPLC with the peak showing the λmax of 228 nm. The melting point and λ max and according to USP 741 confirm the labelled on the drug sample of PTX [44].

5.2.2 Effect of solvent

Drug loading is mainly based on the adsorptive properties of MSNs. Both hydrophilic and hydrophobic cargos can be incorporated into the pores of MSNs. Owing to their large pore volume, MSNs inherently possess greater loading capacity compared to other carriers. To evaluate the feasibility of MSN to load the hydrophobic PTX in different solvents, water, ethanol, DMSO and dichloromethane were chosen. The polarity parameters of water, ethanol, DMSO and dichloromethane were 10.2, 7.8, 7.2, and 3.4 respectively. As shown in Table 4, the drug loading capacity increased with the decrease of the solvent polarity parameter, and MSN had the highest drug loading content of 24.6%. This was most likely because the less polar solvent did not compete with the highly hydrophobic PTX molecule to absorb on the surface of MSN, hence drug loading content was significantly increased.

Table 4: Loading capacity at different solvents

Solvent	Polarity	Loading capacity (%)
Water	10.2	10.2
Ethanol	7.8	11.6
DMSO	7.2	22.8
Dichloromethane	3.4	24.6

5.2.3 Drug loading periods

To determine the optimal time for PTX loading, different drug loading periods (1, 2, 4, 8, 16, 24) h at 25 ºC and 400 rpm were utilized to investigate the adsorption equilibrium time of the drug when the drug loading processed in dichloromethane for both S-MSNs and L-MSNs. As depicted in Figure 12, the drug loading content gradually increased with the increase of the loading period within 6 h about 18.6% for S-MSNs and 24.6% for L-MSNs. As the loading period increased to 24 h, the drug loading content was still stay constant, indicating that drug adsorption on the surface of MSN had reached equilibrium at 6 hr., Hence, the optimal drug loading time was 6 h. The loading of PTX was driven by diffusion where due to concentration

gradient PTX diffused into a porous structure with lower concentration from a bulk of solution with higher concentration. A load of drugs with MSNs depends on the size of the pore, the PTX loading capacity (PTX/LC) and the PTX loading efficiency (PTX/LE) were calculated using a HPLC as two types of MSNs calculated with the help of the calibration curve for the investigation of the carrier's ability.

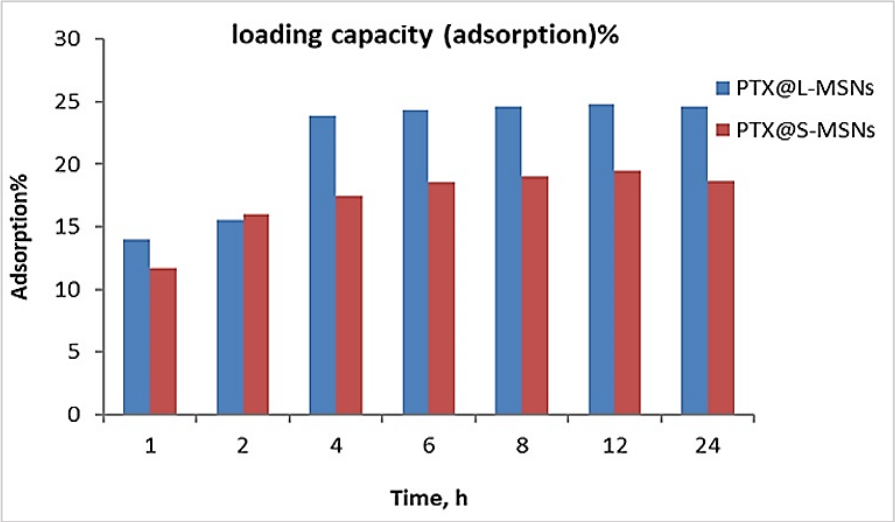

Figure 12: Effect of period time on loading capacity

As shown in Table 5, LC% in L-MSNs is greater than S-MSNs because the surface area of S-MSNs is smaller than L-MSNs and of the larger size of L-MSNs, which provided much more free hydroxyls group than S-MSNs, capable of forming hydrogen bonds with PTX.

Table 5: MSN loading efficiency and loading capacity percentage in dichloromethane

Nanocarriers	Loading efficiency (%)	Loading capacity (%)
L-MSNs	21	24.6
S-MSNs	10.4	18.6

5.3 In vitro drug release

5.3.1 Calibration curve

Calibration curve of PTX: Figure 13 shows the calibration curve of PTX in methanol. The plotting of area against concentrations resulted in a straight line. The square correlation coefficients (R2) were found to be (0.9996). This means that the calibration curve complied with the law of Beer in the range of concentrations used.

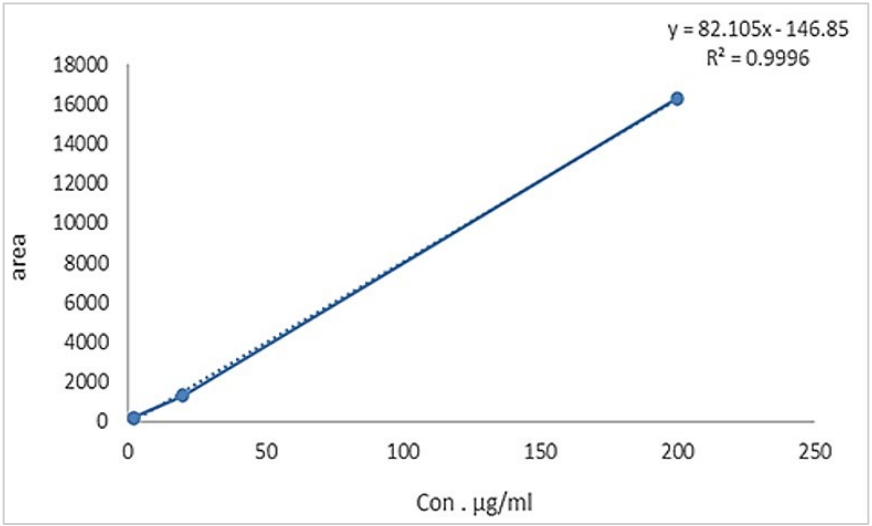

Figure 13: Calibration curve of PTX in methanol by HPLC

5.3.2 In vitro drug release

To investigate the drug release profile of PTX@S-MSNs, and PTX@L-MSNs, compared with free PTX the in vitro drug release was carried out at two pH conditions, pH = 7.4 and 5.5 as representative of physiological and cancer environment

conditions. This studied in PBS containing 0.1% (v/v) Tween 80 at 37 °C. All the release rates of PTX from loaded MSNs were much faster than that of pure drug as shown in Figure 14.

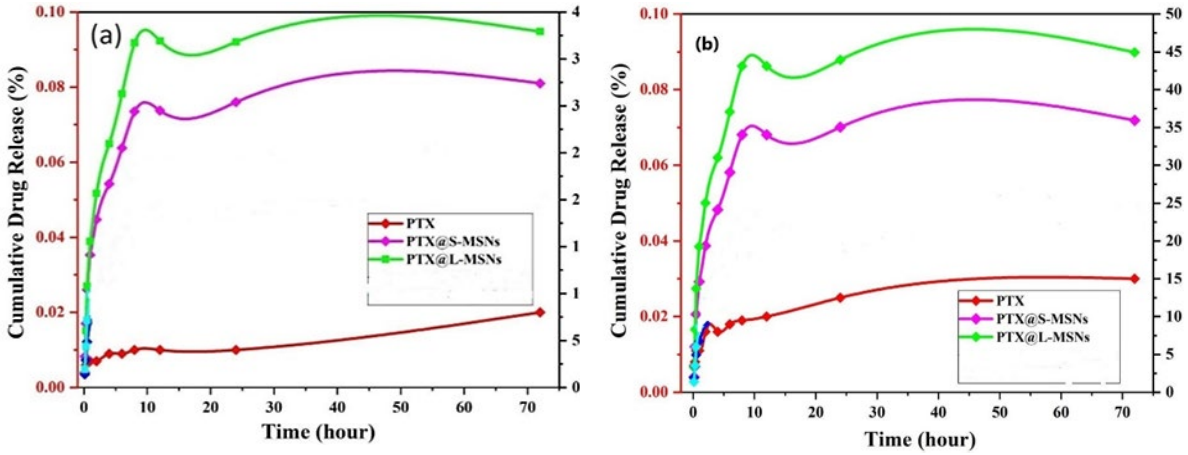

Figure 14: PTX release from samples at PH (a:7.4, b:5.5)

All the in vitro drug releases of loaded MSNs exhibited biphasic drug release patterns with burst release at the initial stage and prolonged release afterward. The initial burst release of PTX which could be beneficial for quickly reaching the effective treatment concentration, was due to the presence of PTX in the external pores of MSNs. PTX in the pores inside MSNs were released slowly into the release medium and maintained effective concentration. Compared with the long-term and sustained increasing drug release of PTX@S-MSNs and PTX@L-MSNs with free PTX, the improved dissolution of PTX from mesoporous silica nanoparticles is the crystal transition from ordered to disordered caused by spatial confinement within a nanosized pore.

The PTX release from MSNs at pH 5.5 was faster than pH 7.4, and the release of PTX at pH 7.4 during the first 8 hr. was 37%, and 33%, for PTX@L-MSNs, and PTX@S-MSNs, respectively, the release of PTX at PH 5.5 during the first 8 hrs. was 46%, 38%, 26%, and 21% for PTX@L-MSNs and PTX@S-MSNs, respectively, which can be considered as a burst release. The release in acidic media at pH 5.5 is better than another pH, so this indicates that there is no release of the drug primarily in circulation or say premature release from MSN unless arriving and is engulfed by cancer cells, as a result, decreases the side effect of the drug. In simple, the formulated DDS displays a pH-sensitive and durable PTX release nature, which is crucial for specific and efficient cancer treatment. Since a tumor tissue is more acidic than normal tissues, the optimal pH-sensitive mechanism is that in normal tissues, drugs are not released and suppress harmful side effects but may be released to improve the treatment of tumor tissues.

6. Conclusion

In this work the following main conclusions can be drawn:

1) Two types of ordered MSNs (small and large pores), with acceptable surface area and appropriate pore sizes, have been synthesized successfully by sol-gel method using TEOS as a source of silica, CTAB surfactant, and mesitylene as pores expender. The findings indicated that monodispersed MSNs with specific surface area for S-MSNs (424.27 m^2/g) and L-MSNs (686.84 m^2/g). The pore size of S-MSNs and L-MSNs was 2.5 nm and 3.2 nm, respectively. we found that pore size increased with an increase in Mesitylene (swelling agent) mixing time at 3 h After that time there was no increase in pore size.
2) MSNs were effectively prepared that provided the ability to encapsulate antitumor drug PTX with high load capacity in their mesopores. the MSNs used to load the hydrophobic PTX in different solvents, the drug loading capacity increased with the decrease of the solvent polarity parameter. The drug loading efficiency of PTX increased with increasing contact time and after 6 hr., it has become almost constant, for both S-MCMs and L-MCMs dosage, and maximum drug loading efficiency for PTX for -MCMs and L-MCMs (24% and 18.6%) respectively.
3) The PTX release in acidic media at pH 5.5 is better than pH 7.4 and as a result, reduces side effects from the drug Since tumor tissue is more acidic than normal tissue, but may be released to improve treatment in tumor tissue.

Author contributions

Conceptualization, **H. Abbood**; **A. Abdul-Hamead; and F. Othman**; data curation, **H. Abbood**; **A. Abdul-Hamead; and F. Othmanand**.; formal analysis, **H. Abbood**; **A. Abdul-Hamead; and F. Othmanand**; investigation, **H. Abbood**; **A. Abdul-Hamead; and F. Othmanand**.; methodology, **H. Abbood**; **A. Abdul-Hamead; and F. Othman**.; project administration, **A. Abdul-Hamead; and F. Othman**. resources, **H. Abbood**.; software, **H. Abbood**.; supervision, **A. Abdul-Hamead; and F. Othman**.; validation, **H. Abbood**; **A. Abdul-Hamead; and F. Othman**.; visualization, **H. Abbood**; **A. Abdul-Hamead; and F. Othman**.; writing—original draft preparation, **H. Abbood**.; writing—review and editing, **H. Abbood**; **A. Abdul-Hamead; and F. Othman.** All authors have read and agreed to the published version of the manuscript.

Funding

This research received no specific grant from any funding agency in the public, commercial, or not-for-profit sectors.

Data availability statement

The researcher took the information, and the rest of the data is in the author's thesis in the Department of Materials Engineering, University of Technology library.

Conflicts of interest

The authors declare that there is no conflict of interest.

References

[1] C. Zhang, L. Yan, X. Wang, S. Zhu, C. Chen, Z. Gu, and Y. Zhao, Progress, challenges, and future of nanomedicine, Nano Today, 35 (2020) 101008. https://doi.org/10.1016/j.nantod.2020.101008

[2] T. Sahu, Y. K. Ratre, S. Chauhan, L. V. K. S. Bhaskar, M. P. Nair, and H. K. Verma, Nanotechnology based drug delivery system: Current strategies and emerging therapeutic potential for medical science, J. Drug Delivery Sci. Technol., 63 (2021) 102487. https://doi.org/10.1016/j.jddst.2021.102487

[3] M. C. Garnett, and P. Kallinteri, Nanomedicines and nanotoxicology: some physiological principles, Occup Med., 56 (2006) 307-311. https://doi.org/10.1093/occmed/kql052

[4] R. M. Samarasinghe, R. K. Kanwar, and J. R. Kanwar, The role of nanomedicine in cell-based therapeutics in cancer and inflammation, Int. J. Mol. Cell. Med., 1 (2012) 133-144.

[5] S. C. Thomas, P. K. Mishra, and S. Talegaonkar, Ceramic nanoparticles: fabrication methods and applications in drug delivery, Curr. Pharm. Des., 21 (2015) 6165-6188. http://dx.doi.org/10.2174/1381612821666151027153246

[6] A. A. Yaqoob, H. Ahmad, T. Parveen, A. Ahmad, M. Oves, I. M. Ismail et al., Recent advances in metal decorated nanomaterials and their various biological applications: A review, Front. Chem, 8 (2020) 341. https://doi.org/10.3389/fchem.2020.00341

[7] S. Soares, J. Sousa, A. Pais, and C. Vitorino, Nanomedicine: principles, properties, and regulatory issues, Front. Chem, 6 (2018) 360. https://doi.org/10.3389/fchem.2018.00360

[8] K. S. Jadhav, P. S. Dumbare, and V. V. Pande, Mesoporous silica nanoparticles (MSN): a nanonetwork and hierarchical structure in drug delivery, J. Nanomed. Res., 2 (2015) 1-8. http://dx.doi.org/10.15406/jnmr.2015.02.00043

[9] D. Lombardo, M. A. Kiselev, M. A., and M. T. Caccamo, Smart nanoparticles for drug delivery application: development of versatile nanocarrier platforms in biotechnology and nanomedicine, J. Nanomater., 2019 (2019) 1-26. https://doi.org/10.1155/2019/3702518

[10] M. Mirzaei, M. B. Zarch, M. Darroudi, K. Sayyadi, S. T. Keshavarz, J. Sayyadi, et al., Silica mesoporous structures: Effective nanocarriers in drug delivery and nanocatalysts, Appl. Sci., 10 (2020) 7533. https://doi.org/10.3390/app10217533

[11] S. Kwon, R. K. Singh, R. A. Perez, E. A. Abou Neel, H. W. Kim, et al., Silica-based mesoporous nanoparticles for controlled drug delivery, J. Tissue Eng., 4 (2013). https://doi.org/10.1177/2041731413503357

[12] N. Iturrioz-Rodríguez, M. A. Correa-Duarte, and M. L. Fanarraga, Controlled drug delivery systems for cancer based on mesoporous silica nanoparticles, Int. J. Nanomed., (2019) 3389-3401. https://doi.org/10.2147/IJN.S198848

[13] G. Liu, L. Yang, G. Chen, F. Xu, F. Yang, et al., A Review on drug delivery system for tumor therapy, Front. Pharmacol., 12 (2021) 735446. https://doi.org/10.3389/fphar.2021.735446

[14] S. Basavaraj and G. V. Betageri, Can formulation and drug delivery reduce attrition during drug discovery and development—review of feasibility, benefits and challenges, Acta Pharm. Sin. B, 4 (2014) 3-17. https://doi.org/10.1016/j.apsb.2013.12.003

[15] S. Ezrahi, A. Aserin, and N. Garti, Basic principles of drug delivery systems– the case of paclitaxel, Adv. Colloid Interface Sci., 263 (2019) 95-130. https://doi.org/10.1016/j.cis.2018.11.004

[16] R. C. Alves, R. P. Fernandes, J. O. Eloy, H. R. N. Salgado, and M. Chorilli, Characteristics, properties and analytical methods of paclitaxel: a review, Crit. Rev. Anal. Chem., 48 (2018) 110-118. https://doi.org/10.1080/10408347.2017.1416283

[17] F. Raza, H. Zafar, M. W. Khan, A. Ullah, A. U. Khan, et al., Recent advances in the targeted delivery of paclitaxel nanomedicine for cancer therapy, Mater. Adv., 3 (2022) 2268-2290. https://doi.org/10.1039/D1MA00961C

[18] M. Ghaferi, M. K. M. Esfahani, A. Raza, S. Al Harthi, H. E. Shahmabadi, S. E. Alavi, Mesoporous silica nanoparticles: Synthesis methods and their therapeutic use-recent advances, J. Drug Targeting, 29 (2021) 131-154. https://doi.org/10.1080/1061186x.2020.1812614

[19] C. Bharti, U. Nagaich, A. K. Pal, and N. Gulati, Mesoporous silica nanoparticles in target drug delivery system: A review, Int. J. Pharm. Invest., 5 (2015) 124. https://doi.org/10.4103/2230-973x.160844

[20] K. B. Seljak, P. Kocbek, M. Gašperlin, Mesoporous silica nanoparticles as delivery carriers: An overview of drug loading techniques, J. Drug Delivery Sci. Technol., 59 (2020) 101906. https://doi.org/10.1016/j.jddst.2020.101906

[21] M. Yu, W. Yuan, D. Li, A. Schwendeman, and S. P. Schwendeman, Predicting drug release kinetics from nanocarriers inside dialysis bags, J. Controlled Release, 315 (2019) 23-30. https://doi.org/10.1016/j.jconrel.2019.09.016

[22] S. J. Wallace, J. Li, R. L. Nation, and B. J. Boyd, Drug release from nanomedicines: selection of appropriate encapsulation and release methodology, Drug Delivery Transl. Res., 2 (2012) 284-292. https://doi.org/10.1007/s13346-012-0064-4

[23] C. Mbakaan, I. Ahemen, A. N. Amah, A. D. Onojah, and L. Koao, White-light emitting Dy3+-doped amorphous SiO_2 nanophosphors derived from rice husk, Appl. Phys. A, 124 (2018) 741. https://doi.org/10.1007/S00339-018-2156-6

[24] I. Karapanagiotis, S. Sotiropoulou, S. Vasileiadou, E. Karagiannidou, D. Mantzouris, and P. Tsiamyrtzis, (2018). Shellfish purple and gold threads from a Late Antique tomb excavated in Thessaloniki, ARACHNE, 5 (2018) 64-77.

[25] E. K. Richman, C. B. Kang, T. Brezesinski, and S. H. Tolbert, Ordered mesoporous silicon through magnesium reduction of polymer templated silica thin films, Nano Lett., 8 (2008) 3075-3079. https://doi.org/10.1021/nl801759x

[26] K. H. Kim, D. J. Lee, K. M. Cho, S. J. Kim, J. K. Park, and H. T. Jung, Complete magnesiothermic reduction reaction of vertically aligned mesoporous silica channels to form pure silicon nanoparticles, Sci. Rep., 5 (2015) 9014. https://doi.org/10.1038/srep09014

[27] Z. Jiang, C. Li, C. S. Hao, K. Zhu, and P. Zhang, An easy way for preparing high performance porous silicon powder by acid etching Al–Si alloy powder for lithium ion battery, Electrochim. Acta, 115 (2014) 393-398. https://doi.org/10.1016/j.electacta.2013.08.123

[28] R. J. Robson, and E. A. Dennis, The size, shape, and hydration of nonionic surfactant micelles. Triton X-100, J. Phys. Chem., 81 (1977) 1075-1078. https://doi.org/10.1021/j100526a010

[29] H. Yin, P. Zheng, J. Zhao, and W. Shen, The inter-micellar interaction enthalpies of DTAB/TX100 mixed micelles and their structural transitions, Soft Matter, 13 (2017) 5888-5896. https://doi.org/10.1039/C7SM00912G

[30] J. M. Borreguero, P. A. Pincus, B. G. Sumpter, and M. Goswami, Unraveling the agglomeration mechanism in charged block copolymer and surfactant complexes, Macromolecules, 50 (2017) 1193-1205. https://doi.org/10.1021/acs.macromol.6b02319

[31] V. H. Nguyen, C. M. Vu, H. Choi, and B. X. Kien, Nanosilica extracted from hexafluorosilicic acid of waste fertilizer as reinforcement material for natural rubber: Preparation and mechanical characteristics, Materials, 12 (2019) 2707. https://doi.org/10.3390/ma12172707

[32] N. T. Nguyen-Thi, L. P. Pham Tran, N. T. T. Le, M. T. Cao, T. N. Tran, et al., The engineering of porous silica and hollow silica nanoparticles to enhance drug-loading capacity, Processes, 7 (2019) 805. https://doi.org/10.3390/pr7110805

[33] G. Lucovsky, J. Yang, S..S Chao, J.E. Tyler, W. Czubatyj, Oxygen-bonding environments in glow-discharge-deposited amorphous silicon-hydrogen alloy films, Phys. Rev. B, 28 (1983) 3225-3233. https://doi.org/10.1103/PhysRevB.28.3225

[34] P. Gupta, V.L. Colvin, S.M. George, Hydrogen desorption kinetics from monohydride and dihydride species on silicon surfaces, Phys. Rev. B, 37 (1988) 8234-8243. https://doi.org/10.1103/PhysRevB.37.8234

[35] P. Gupta, A.C. Dillon, A.S. Bracker, S.M. George, FTIR studies of H_2O and D_2O decomposition on porous silicon surfaces, Surf. Sci., 245 (1991) 360-372. https://doi.org/10.1016/0039-6028(91)90038-T

[36] H. Park, A.A. Stramel, D.A. Harju, S.M. Weiss, J.H. Dickerson, A novel method of photonic band-gap lithography of porous silicon heterostructures, Active Photonic Crystals, 6640 (2007) 41-46. https://doi.org/10.1117/12.736193

[37] Z. Wang, Y. Tian, H. Zhang, Y. Qin, D. Li, L. Gan, F. Wu, Using hyaluronic acid-functionalized pH stimuli-responsive mesoporous silica nanoparticles for targeted delivery to CD44-overexpressing cancer cells, Int. J. Nanomed.,11 (2016) 6485-6497. https://doi.org/10.2147/IJN.S117184

[38] P.T. Ha, H.N. Nguyen, H.D. Do, Q.T. Phan, M.N.T. Thi, X.P. Nguyen, M.N.H. Thi, M.H. Le, L.T. Nguyen, Targeted drug delivery nanosystems based on copolymer poly (lactide)-tocopheryl polyethylene glycol succinate for cancer treatment, Adv. Nat. Sci: Nanosci. Nanotechnol., 7 (2016) 015001. https://dx.doi.org/10.1088/2043-6262/7/1/015001

[39] T.S.R. Devi, S. Gayathri, FTIR and FT-Raman spectral analysis of paclitaxel drugs, Int. J. Pharm. Sci. Rev. Res., 2 (2010) 106-110.

[40] C. Li, C. Liu, K. Ahmed, Z. Mutlu, Y. Yan, I. Lee, M. Ozkan, C.S. Ozkan, Kinetics and electrochemical evolution of binary silicon–polymer systems for lithium ion batteries, RSC Adv., 7 (2017) 36541-36549. https://doi.org/10.1039/C7RA06023H

[41] V.V. Poltavets, K.A. Lokshin, M. Greenblatt. Isothermal section of the $Na_{0.3}CoO_2$-H_2O phase diagram at 22 °C from 11 to 100% relative humidity, Solid State Sci., 7 (2005) 1312-1316. https://doi.org/10.1016/j.solidstatesciences.2005.05.001

[42] R.T. Liggins, W.L. Hunter, H.M. Burt, Solid-state characterization of paclitaxel, J. Pharm. Sci., 86 (1997) 1458-1463. https://doi.org/10.1021/js9605226

[43] K. Priyadarshini, A.U. Keerthi, Paclitaxel against cancer: a short review, Med. Chem., 2 (2012) 139-141. https://doi.org/10.4172/2161-0444.1000130

[44] T.S.R. Devi, S. Gayathri, Estimation of paclitaxel drugs by HPLC method, Der Pharma Chemica, 2 (2010) 109-115.